CrystEngComm

Cite this: *CrystEngComm*, 2012, **14**, 7015–7024

www.rsc.org/crystengcomm

PAPER

Anion driven modulation of magnetic intermolecular interactions and spin crossover properties in an isomorphous series of mononuclear iron(III) complexes with a hexadentate Schiff base ligand†

Ivan Nemec,*[a] Radovan Herchel,[a] Ivan Šalitroš,[bd] Zdeněk Trávníček,[a] Ján Moncoľ,[b] Hartmut Fuess,[c] Mario Ruben[d] and Wolfgang Linert[e]

Received 30th May 2012, Accepted 21st July 2012
DOI: 10.1039/c2ce25862e

A series of spin crossover iron(III) complexes with the general composition [Fe(4OH-L6)]X (H_2-4OH-L6 = 1,8-bis(4-hydroxysalicylaldiminato)-3,6-diazaoctane; X = Cl, **1a**; Br, **1b**; I, **1c**) was prepared. A combination of the results following the single crystal X-ray analysis, infrared and EPR spectroscopy, and temperature dependent magnetic experiments revealed that the Fe(III) atoms occur in the low-spin state below room temperature and the crystal structures of the complexes involve rich networks of non-covalent intermolecular contacts resulting in two-dimensional supramolecular structures. Alterations in the halide anions influence the strength of the non-covalent contacts and affect the magnetic properties of the studied complexes. The antiferromagnetic exchange interaction between the non-covalently bound cations is the most obvious in the case of **1a** and it weakens with the growing anionic volume of X. The 1D and 2D spin Hamiltonian models were applied to quantitatively extract the information about the intermolecular magnetic exchange (fit on 1D infinite chain gives $J(\mathbf{1a}) = -2.86\ \mathrm{cm}^{-1}$, $J(\mathbf{1b}) = -2.02\ \mathrm{cm}^{-1}$, $J(\mathbf{1c}) = -1.16\ \mathrm{cm}^{-1}$). Furthermore, gradual spin crossover behaviour for all of the compounds of the series was observed above room temperature in the solid state. Spin crossover accompanied by thermochromism was also demonstrated by EPR experiments in solution.

Introduction

The coordination compounds exhibiting spin crossover (SCO) phenomena have been the subject of research for almost 80 years from their discovery.[1] SCO is considered to be an entropy driven, unimolecular reaction (*resp*. transition) between the low-spin (LS) and high-spin (HS) states of the $3d^4$–$3d^7$ coordination compounds exposed to an external perturbation such as temperature, pressure, a magnetic field change, and light irradiation.[2] The iron (II) and iron(III) complexes are the most widely and thoroughly explored SCO compounds,[3] especially the iron(II) compounds such as [Fe(bpy)$_2$(NCS)$_2$] or [Fe(phen)$_2$(NCS)$_2$] (bpy = 2,2′-bipyridine, phen = 1,10′-phenanthroline).[4]

One of the most studied series of iron(III) SCO compounds is represented by the complexes with the hexadentate Schiff-base ligand H_2-L6 resulting from the reactions of variously substituted aromatic 2-hydroxy-aldehydes with triethylenetetramine. (H_2-L6 = N,N′-Bis[2-(salicylideneamino)ethyl]ethane-1,2-diamine, see Fig. 1). Common abbreviations found in the literature are H_2saltrien, H_2sal$_2$trien, herein, the abbreviation X-L6 will be used, where X marks the substitution of the aromatic rings). Concerning the SCO phenomenon, several interesting results

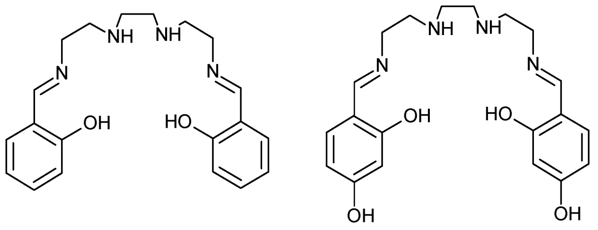

Fig. 1 Drawings of H_2-L6 (left) and H_2-4OH-L6 (right).

---

[a] *Regional Centre of Advanced Technologies and Materials, Department of Inorganic Chemistry, Faculty of Science, Palacký University, 17. Listopadu 12, CZ-77146, Olomouc, Czech Republic. E-mail: ivan.nemec@upol.cz*
[b] *Institute of Inorganic Chemistry, Slovak University of Technology, Radlinského 9, SK, 812 37, Bratislava, Slovakia. E-mail: ivan.salitros@stuba.sk*
[c] *Materials Science, Darmstadt University of Technology, D-64287, Darmstadt, Germany. E-mail: hfuess@tu-darmstadt.de*
[d] *Karlsruhe Institute of Technology (KIT), Institute of Nanotechnology, Hermann-von-Helmholtz-Platz 1, 76344, Eggenstein-Leopoldshafen, Germany. E-mail: mario.ruben@kit.edu*
[e] *Institute of Applied Synthetic Chemistry, Vienna University of Technology, 1060, Vienna, Austria. E-mail: wlinert@mail.zserv.tuwien.ac.at*

† Electronic supplementary information (ESI) available: ORTEP graphics of the title compounds, thermogravimetric data, and details of the magnetic and EPR data analysis. CCDC reference numbers 884404–884406. For ESI and crystallographic data in CIF or other electronic format see DOI: 10.1039/c2ce25862e

were achieved within this series. The compound of [Fe(L6)][Ni(dmit)$_2$] (dmit^{2-} = 2-thioxo-1,3-dithiole-4,5-dithiolate) exhibits abrupt SCO with wide thermal hysteresis (30 K wide)[5] which is accompanied with a large reorganization within the crystal structure. Generally speaking, such compounds may serve as precursors for the preparation of hybrid materials combining the SCO and electrical conductivity properties.[6] Another interesting combination of physical properties was achieved by insertion of the [Fe(L6)]$^+$ cation between the ferromagnetic bimetallic oxalate layers.[7] Both magnetic phenomena are observed, though the spin transition is of a gradual character. The [Fe(3MeO-L6)]$^+$ derivative was intercalated within the MnPS$_3$ layered magnet and the observed spin transition is gradual when the sample is untreated. After the removal of co-intercalated water molecules, magnetic behaviour is affected significantly, *i.e.* a broad hysteresis appears.[8]

As was reported in 2008,[9] the various magnetic behaviours of the [Fe(X-L6)]$^+$ analogues can be explained on the basis of the molecular shape flexibility (a conformation of the coordinated ligand), especially the varying angle between the least square planes of the phenolate rings (α, usually lying in the range of 60–125°), which seems to be an important and useful parameter. Despite a few exceptions, it can be generalized that the LS compounds adopt the ligand conformation with the α angle of 60–70° approximately, while the L6^{2-} ligand is structurally more variable in the HS compounds and adopts the conformation with the α angle bigger than 90°. Compounds with the value of the α angle close to 90° are likely to undergo SCO. The intermolecular interactions present in the crystal structure cause cooperative behaviour, which is responsible for the abruptness of the transitions, or even for the occurrence of thermal hysteresis.[2,10]

In order to achieve systems rich in hydrogen bonding,[11] we decided to prepare the 4-hydroxy derivative of L6^{2-} (4OH-L6 dianion) and to use it as a ligand (Fig. 1).

Herein, we report the synthesis, X-ray structures, magnetic and spectroscopic properties of a series of isostructural compounds with the general formula [Fe(4OH-L6)]X (X = Cl$^-$, Br$^-$, I$^-$). Physical properties are discussed with respect to the alteration of the size and hydrogen bonding acceptor properties of the halide anion.

Results and discussion

Crystal structures

The compounds involved into the studied series are isomorphous and crystallize in the *P*2/*c* space group. Crystal data and structure refinements can be found in Table 1. The crystallographically independent parts of the structures consist of half of the [Fe(4OH-L6)]$^+$ cations and half of the halide anions of Cl$^-$ (**1a**), Br$^-$ (**1b**) or I$^-$ (**1c**) (ORTEP plots of **1a–c** are provided in ESI,† Fig. S1). The iron(III) atoms as well as the halogen atoms lie in the special positions on the two-fold axis and are constrained with the occupation factors equal to 0.5. The bond lengths within the FeN$_4$O$_2$ chromophore as well as the shape of the cation parameterized by α (Table 2, α (**1a–c**) = 62.3–62.7°)[9] correspond to the low spin character of the iron centre. The observed α values are similar to those which were found in the previously reported [Fe(L6)]$^+$ compounds purely in the LS state.[12]

The crystal structures of the polymorphs (Fig. 2) are formed by the layers of supramolecular one-dimensional zig-zag chains of the {[Fe(4OH-L6)]$^+$}$_n$ cations stacked by the

Table 1 Selected crystal data and structure refinements for **1a–c**

	1a	**1b**	**1c**
Crystal system	Monoclinic	Monoclinic	Monoclinic
Space group	P2/c	P2/c	P2/c
a/Å	9.660(9)	9.9131(4)	10.168(3)
b/Å	9.651(9)	9.6378(4)	9.680(3)
c/Å	13.590(12)	13.7350(7)	13.871(4)
β	128.17(5)	129.198(3)	130.17(2)
V/Å^3	996.1(16)	1016.95(8)	1043.2(6)
T/K	298	298	160
ρ_{calc}/g.cm^{-3}	1.586	1.698	1.806
μ/mm^{-1}	0.928	2.742	2.238
goodness of fit	0.980	1.036	1.107
data/restraints/parameters	1763/0/138	1800/0/138	1844/0/138
r_{int}/r_σ	0.0342/0.0487	0.0246/0.0270	0.0736/0.0528
$R_1{}^a$/w$R_2{}^b$(all data)	0.0570/0.0657	0.0416/0.0800	0.0620/0.1540
$R_1{}^a$/w$R_2{}^b$($I > 2\sigma(I)$)	0.0306/0.0604	0.0297/0.0774	0.0830/0.1540
CCDC number	884404	884405	884406

[a] $R_1 = \sum (|F_o| - |F_c|)/\sum|F_o|$. [b] w$R^2 = \{\sum[w(F_o{}^2 - F_c{}^2)^2]/\sum[w(F_o{}^2)^2]\}^{1/2}$.

Table 2 Selected non-covalent contact parameters (Å, °) in the crystal structures of **1a–c**

	T/K	d(Fe–N)$_{am}$	d(Fe–N)$_{im}$	d(Fe–O)	d(N2···O2)	d(O2···X)	$d(\pi-\pi)^a$	α/°	Σ/°^{b}
1a	298	2.011 (3)	1.922 (3)	1.877 (2)	3.004 (4)	3.042 (3)	3.751(2)	62.3	45.4
1b	298	2.016 (2)	1.924 (2)	1.877 (2)	2.981 (2)	3.188 (3)	3.876 (3)	62.3	51.2
1c	160	2.011 (5)	1.932 (5)	1.881 (4)	2.973 (6)	3.344 (8)	4.046 (6)	62.7	50.2

[a] Centroid–centroid distance. [b] Octahedral distortion calculated as $\sum_{i}^{12} = |90 - \alpha_i|$, where α_i stands for 12 *cis* angles of the coordination polyhedron.

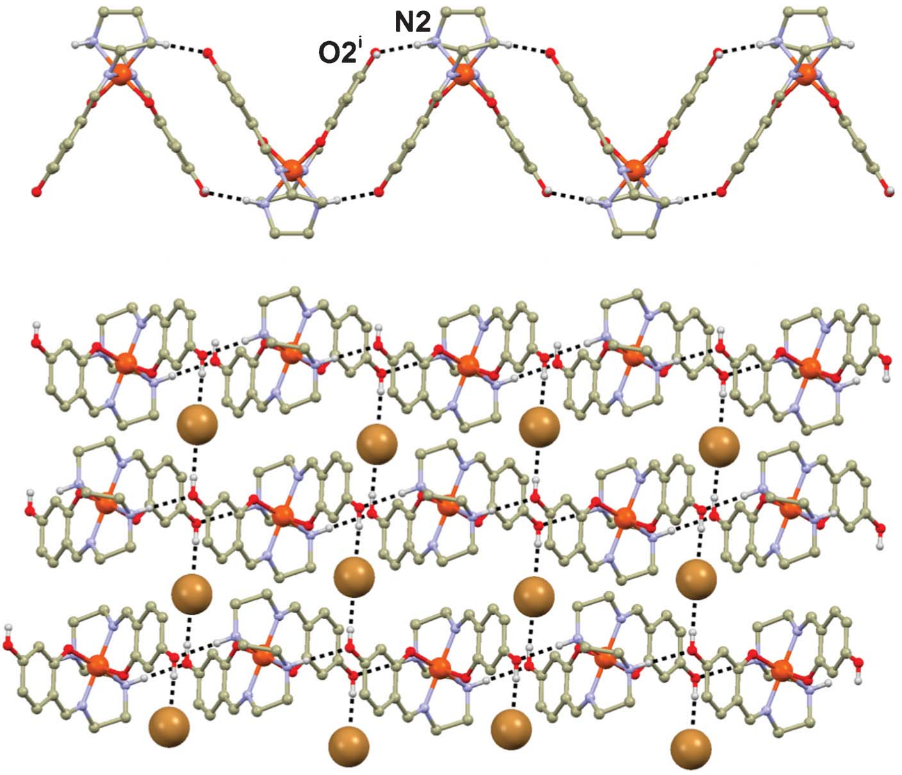

Fig. 2 (top) Projection (along with the *c* axis) of the one-dimensional chain fragment in [Fe(4OH-L6)]X; (bottom) the rich system of hydrogen bonding in the two-dimensional layered structure of [Fe(4OH-L6)]X. The halide anions are displayed in brown using the space-filling mode with the van der Waal's radii set up at 0.5 for clarity. In both pictures, the hydrogen atoms (except for those involved in hydrogen bonding) are omitted for clarity and hydrogen bonding is displayed as black dashed lines.

N2–H(NH)···O2^i [Symmetry code: (i) $x - 1, -y - 1, z - 1/2$] hydrogen bonds between the amino nitrogen atoms (N2, donor) and peripheral hydroxy oxygen atoms (O2) with the d\{N2···O2^i\} distances in the range of 2.96–3.00 Å (Table 2). The hydrogen-bonding angles <\{N2–H(NH)–O2^i\} are in the narrow range of 170–179°. The pair of the N2–H(NH)···O2^i hydrogen bonds link two neighbouring [Fe(4OH-L6)]$^+$ cations into the $R_2^2(16)$ ring structure, thus creating the infinite zig-zag chains.[13] The chain structure is supported by the offset π-stacked π–π stacking interactions[14] between the phenyl rings of the adjacent cations. The plane–plane distances are found to be in the range of 3.36–3.52 Å, and the centroid–centroid distances in the range of 3.74–4.07 Å (Table 2). These values are in agreement with the parameters reported for the offset π-stacked interactions.[14]

The zig-zag chains are interconnected by the O2–H(OH)···X1^{ii} hydrogen bonds [symmetry code: (ii) x, y, z] between the hydroxy groups and halide anions, which form the $R_6^4(22)$ ring.[13]

With the growing volume of the halide anion, the significant changes in the lengths of intermolecular contacts (Fig. 3, middle) are observed. The centroid–centroid distances of the stacked aromatic rings, as well as the lengths of the hydrogen bonds between the peripheral hydroxy groups and the halide anions, grow significantly with the anion substitution. These changes can be explained on the basis of the growing anion volume and lowering of the electronegativity in a series from chloride to iodide. Due to these reasons the big iodide anion is a much weaker acceptor of a hydrogen bond in comparison with the smaller and more electronegative chloride anion. Therefore, the iodide anion provides weaker and longer hydrogen bonds (Cl: d\{O2···Cl1\} = 3.029(3) Å at 100 K, I: d\{O2···I1\} = 3.351(4) Å).[15] The hydrogen-bonding angles <\{O2–H(OH)–X1^{ii}\} are in the range of 166–171°, which are typical for moderate and weak O–H···X hydrogen bonds.[16]

The length of the centroid–centroid distance grows with the increasing ionic radius of the halide anions much more significantly than the plane–plane distance (the distance between the least-square planes of the stacked aromatic rings). Thus, it is obvious that the present offset is dependent on the steric influence of the halide anions (Fig. 3, left).

Infrared spectroscopy

The formation of hydrogen bonds affects the vibrational properties of the donor group significantly and usually leads to the observation of a redshift in the frequency of the donor stretching vibration upon the hydrogen bond formation. The frequency of the donor stretching vibration also lowers with the strengthening of the hydrogen bond and thus it can be expected in the series of the isostructural complexes **1a–c** that the compounds with shorter hydrogen bond lengths tend to show lower vibrational frequencies of the appropriate groups.[15]

As was discussed above, the amino and hydroxy donor groups are involved in hydrogen bonding and therefore the attention has to be focused on the wavelength range of 2000–4000 cm^{-1}, where their stretching vibrations can be found. The largest wavelength shift is observed due to the anion substitution for the ν(O–H) vibration. The hydrogen bonded hydroxy group provides

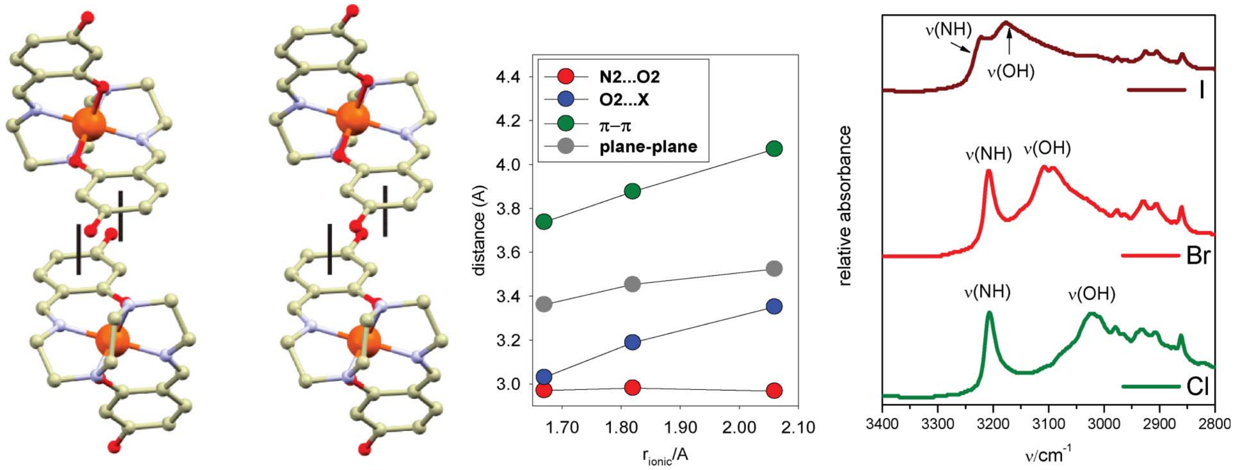

Fig. 3 Structure of the stacked $[\{Fe(4OH\text{-}L6)\}_2]^{2+}$ supramolecular dimers in **1a** (left) and **1c** (right). Hydrogen atoms are omitted for clarity (except for those involved in hydrogen bonding) (left). The offset of the stacked aromatic rings is highlighted by the black lines going out from the ring centroids and perpendicularly to the planes of the aromatic rings. Plots of the dependence of intermolecular contact distance *vs.* anionic volume (middle). Infrared spectra of **1a–c** in the range of 2800–3400 cm^{-1}(right).

superposed peaks broader more than 150 cm^{-1} at the base lines in the spectra of all the compounds (Fig. 3). The largest red shift of the peak maximum is observed in the spectrum of the chloride compound **1a**; ν_{max}(O–H, **1a**) ≈ 3020 cm^{-1}, which is in agreement with the shortest distance of the OH···X hydrogen bond found in **1a** (Table 2) and with the reported correlations between hydrogen bond parameters and vibrational properties.[17] On the contrary, the wavelength of ν_{max}(O–H, **1c**) is observed at a significantly higher frequency, at *ca.* 3180 cm^{-1}. Such a big difference in the maxima of this vibration confirms a large variation in the hydrogen bond strength found between the compounds **1a** and **1c**. The stretching vibration of the amine group is approximately at the same position in all the samples, which is consistent with the structural data, where the length of this contact changes only very slightly upon the anion substitution. All the other vibrations found in the range of 400–2000 cm^{-1} are practically identical, which confirms the isostructurality of the compounds **1a–c**.

EPR spectroscopy

The powder X-band EPR spectra of **1a–c** were recorded at liquid nitrogen and also at room temperature. At T = 77 K, the LS Fe(III) configuration with S = 1/2 is expected by taking into account the Fe–N and Fe–O bond distances (Table 2). In this case, the LS Fe(III) $^2T_{2g}$ term splitting due to spin–orbit coupling and symmetry of the chromophore can be described by the axial (Δ/λ) and tetragonal (V/λ) splitting parameters, respectively, where λ is the spin–orbit splitting parameter within the crystal-field term.[18] The linear combinations of d_{yz}, d_{xz} and d_{xy} orbitals

$$|\pm\rangle = \pm a\left|d_{yz}^{\pm}\right\rangle - ib\left|d_{xz}^{\pm}\right\rangle - c\left|d_{xy}^{\mp}\right\rangle \qquad (1)$$

are used to describe the ground state with the pure spin Hamiltonian formalism for S = 1/2. As EPR does not provide the information about the signs of g-factors, Taylors' equations were used to determine the components of g-tensor and subsequently also the splitting parameters Δ/λ and V/λ.[19] A representative spectrum of **1c** is depicted in Fig. 4. The spectrum is almost axial, with a small rhombic distortion. The EasySpin package[20] was used to simulate all spectra of **1a–c** with three g-factors. The resulting parameters are summarized in Table 3. The own-written program was used to analyse these g-factors by Taylors' equations and to extract the information about the splitting of the d_{yz}, d_{xz} and d_{xy} orbitals (see ESI,† Table S1 for more details).

Two physically reasonable solutions were found when $g_x = -g_1$, $g_y = g_2$ and $g_z = -g_3$ or $g_x = -g_2$, $g_y = g_1$ and $g_z = -g_3$. Resulting negative values of $\Delta/\lambda \approx -10.2$ for **1a–c** signify that the ground state involves the electronic configuration corresponding to $(d_{xz},d_{yz})^4(d_{xy})^1$. Similar values of the axial splitting parameter were found in other analogous Schiff-base iron(III) LS complexes.[21] The relatively small values of $|V/\Delta|$ are in agreement with the presence of the slightly elongated tetragonal bipyramid of the $\{FeN_4O_2\}$ chromophore. In contrast to the liquid nitrogen spectra, the room temperature EPR spectra of **1a–c** are purely axial (Fig. 4), and only the information about $g^{\perp}$ ($g_1 = g_2$) and $g_{\parallel}$(g_3) were determined, see Table 3. Nevertheless, the value of the orbital splitting parameter $\Delta/\lambda \approx -10.1$ is practically the same for all the compounds and for both temperatures. Moreover, the methanolic solutions of **1a–c** were studied by X-band EPR at the same temperatures as powder samples. By dissolving **1a–c**, dark brown solutions were formed at room temperature and on cooling them with liquid nitrogen, a conspicuous change of colour to bright blue occurred, see Fig. 4.

This process was found to be fully reversible and suggests that the spin crossover phenomenon accompanied by thermochromism takes place within the temperature interval of 77–300 K, as reported previously for a group of the $[Fe(X\text{-}L6)]^+$ compounds.[22] Indeed, the frozen solution spectra of **1a–c** were typical for S = 1/2 and they resembled the powder EPR spectra of the solid samples, see Fig. 4. Utilizing the same procedure as explained above, we were able to extract the information about three g-factors and consequently the information about the energy

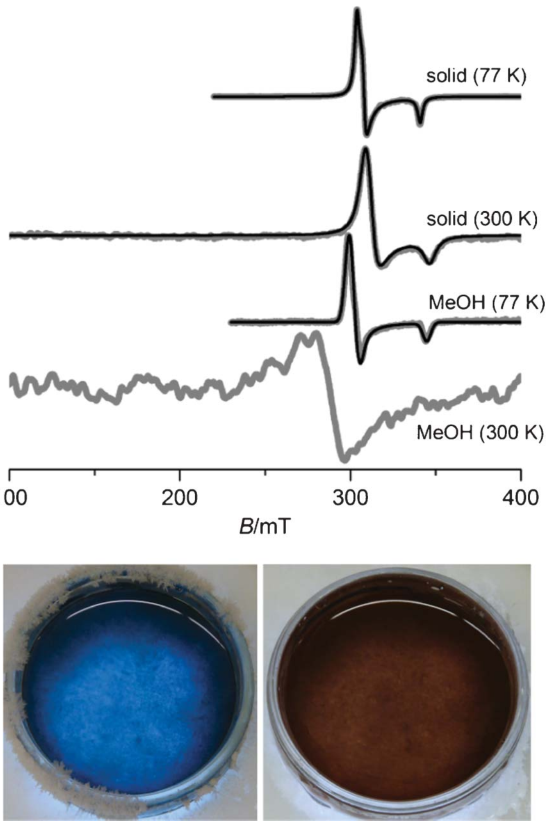

Fig. 4 The powder and solution X-band EPR spectra of **1c** at different temperatures. The experimental data (gray line) and calculated data (black lines) with the parameters given in Table 3 (up). The thermochromism for the methanolic solution of compound **1c** (below right, room temperature, below left, cooled down closely to the freezing point of the solution).

level splitting of the $^2T_{2g}$ term, see Table 3 (see also Table S2, ESI†). It can be concluded that the geometry of the octahedral FeN_4O_2 chromophore is more symmetrical as deduced from the decrease of the energy separation between the (d_{xz}, d_{yz}) and d_{xy} orbitals, $\Delta/\lambda \approx -8.3$, accompanied also by lowering of the $d_{xz} - d_{yz}$ splitting, $|V/\lambda| \approx -0.12$. The room temperature solution spectra of **1a–c** were quite different. Only a very broad signal roughly at $g_{\rm eff} = 2.3$ was observed (Fig. 4), which can be assigned to the small fraction of the LS state of the Fe(III) complexes in the solution. The expected typical HS Fe(III) signal at $g_{\rm eff} = 4.3$–4.7 was not detected, which does not contradict the presumed spin crossover phenomenon manifested by the thermochromism, because similar Fe(III) complexes have been reported, in which the fast-relaxation prevented the observation of the HS state in EPR spectra.[23]

Table 3 The X-band powder and solution EPR parameters for **1a–c**

T/K		g_1	g_2	g_3	lwpp[a]	$\|V/\lambda\|$	Δ/λ	$\|V/\Delta\|$
77	**1a**	2.208	2.172	1.965	2.70	1.73	−10.3	0.169
77	**1b**	2.208	2.173	1.964	2.41	1.66	−10.2	0.163
77	**1c**	2.207	2.177	1.967	1.96	1.44	−10.2	0.141
300	**1a**	2.191		1.965	5.75		−10.1	
300	**1b**	2.192		1.967	6.48		−10.2	
300	**1c**	2.187		1.963	5.87		−10.2	
77	**1a**$^{\rm MeOH}$	2.245	2.212	1.946	4.17	1.04	−8.36	0.125
77	**1b**$^{\rm MeOH}$	2.245	2.210	1.944	4.21	1.10	−8.33	0.132
77	**1c**$^{\rm MeOH}$	2.244	2.216	1.946	4.75	0.88	−8.31	0.105

[a] Line widths for isotropic magnetic-field domain broadening (PP, peak-to-peak, in mT); the Lorentzian broadening was used for powder samples, while the Gaussian broadening was used for methanolic solutions.

Magnetic properties

As can be implied from the green colour of the compounds **1a–c** (typical for the LS compounds of Schiff-base iron(III) complexes with the $\{N_4O_2\}$ donor set)[3], the LS state with S = 1/2 is expected at room temperature for the reported complexes. Indeed, the room temperature effective magnetic moment is 2.16, 2.24 and 2.10 μ_B, for **1a, 1b,** and **1c**, respectively (Fig. 5). These values are a bit higher than the spin-only value ($S = 1/2$, $g = 2$, $\mu_{\rm eff} = 1.73\ \mu_B$), which can be easily explained by two ongoing phenomena: (*i*) a contribution of the orbital angular momentum (*ii*) the spin transition starting near room temperature. In order to confirm that **1a–c** undergo spin crossover, the studied temperature range was set up to 2–450 K using the oven equipment of the SQUID magnetometer (the thermal stability of **1a–c** was verified using the TG/DTA experiments—see ESI,† Fig. S2).

First, let us focus on the low-temperature data analysis. There is a pronounced decrease of $\mu_{\rm eff}/\mu_B$ below 40 K as an indication of the antiferromagnetic interactions among mononuclear entities mediated through non-covalent contacts. The values of the effective magnetic moment at T = 2 K are 1.05, 1.53 and 1.62 μ_B, for **1a, 1b,** and **1c**, respectively. The presence of the antiferromagnetic exchange is also clearly visible in the plots of the isothermal magnetizations measured at T = 2.0 and 4.6 K where a deviation from the Brillouin function for the isolated magnetic centres with S = 1/2 is pronounced. The X-ray analysis confirmed the presence of two types of the intermolecular non-covalent contacts: (i) typical hydrogen bonds of the N–H···O and O–H···X types, and (ii) π–π stacking interactions, resulting in a quasi 2D network. With the intention to quantitatively analyze the intermolecular interactions and to decide whether both types of intermolecular interactions are responsible for the antiferromagnetic interaction, two spin Hamiltonian models were tested for both a 1D chain and 2D network using a finite-size approach. In all these models, the experimental data were truncated up to 250 K to minimize the impact of the spin crossover on the fitted parameters. It must be also noted that the model based on a mean field approximation with the molecular field correction parameter zj[24], failed to properly describe the low-temperature magnetic properties of **1a–c**. First, let us discuss the model of the one-dimensional uniformly coupled chain (S = 1/2). The spin Hamiltonian for the finite-size closed ring with 19 centres was postulated to effectively mimic the infinite chain magnetic properties as

$$\hat{H} = -J\left\{\sum_{i=1}^{18}\vec{S}_i\cdot\vec{S}_{i+1} + \left(\vec{S}_{19}\cdot\vec{S}_1\right)\right\} + \mu_B g B\sum_{i=1}^{19}\hat{S}_{z,i} \qquad (2)$$

The advantage of this approach is that in addition to the susceptibility data, the magnetization data set can also be

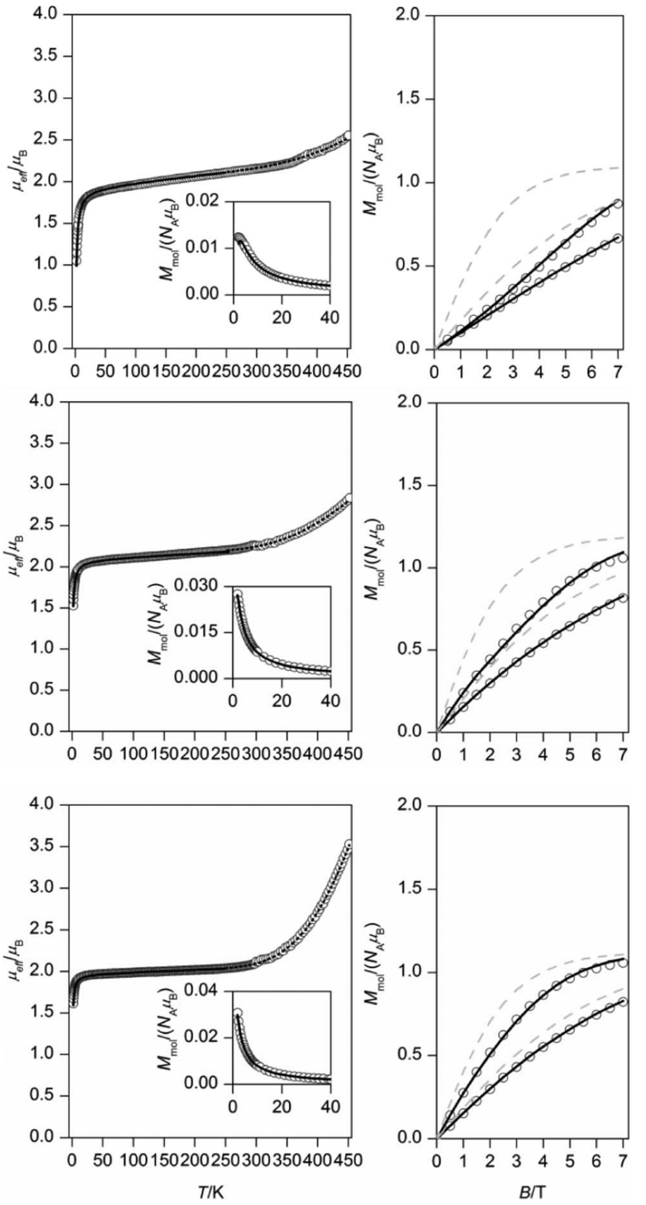

Fig. 5 Magnetic data for **1a** (top), **1b** (middle) and **1c** (bottom). Left: temperature dependence of the effective magnetic moment. Inset: temperature dependence of the magnetization measured at B = 0.1 T. Right: field dependence of magnetization at T = 2.0 and 4.6 K. Empty circles—experimental data; full lines—the best fits to the experimental data *via* the 2D network model (eqn. (5)), dotted lines—the best fits using Ising-like model, dashed lines—the Brillouin functions for non-interacting system. The calculation parameters are listed in Table 4.

treated, as has already been proven.[25] The number of magnetic energy levels is $N = (2S_i + 1)^{19}$ = 524 288. To be able to treat this problem, the coupled spin basis set labelled as $|\alpha SM_S\rangle$, where α represents the intermediate quantum numbers denoting the coupling path, can be efficiently utilized. In the case of the isotropic exchange and only when all local g-factors are equal, the whole interaction matrix can be factorized in accordance with the final spin S. Moreover, it is also sufficient to calculate the zero-field levels only, labelled as $|\alpha S\rangle$, using the irreducible tensor operators.[24] Moreover, the C_2 symmetry of the spin Hamiltonian (the closed ring of spins) can be employed and the symmetry-adapted spin function can be generated using the projection operator method.[26] The classification of the new spin functions is listed in ESI† (Table S3). Now, the largest dimension of the sub-matrix is 12 618 for S = 3/2 and Γ_i = A. Next, the magnetic levels are calculated as $\varepsilon_j(\Gamma_i,\alpha SM_S) = \varepsilon_{i,0}(\Gamma_i,\alpha S) + \mu_B g M_S B$. The resulting energy levels were then used to calculate the molar magnetization as

$$M_{\text{mol}} = N_{\text{A}}\mu_{\text{B}}g\frac{\sum_j M_S \exp[-\varepsilon_j(\Gamma_i,\alpha SM_S)/kT]}{\sum_j \exp[-\varepsilon_j(\Gamma_i,\alpha SM_S)/kT]} \tag{3}$$

The concurrent fitting of both temperature and field dependent datasets resulted in the isotropic exchange parameter J = −2.86 cm^{-1} and g = 2.19 for **1a**—see ESI† (Fig. S3). It is obvious that a quite large intermolecular magnetic interaction of the antiferromagnetic nature is present. The g-value is very similar to the arithmetic average obtained by powder EPR, which is equal to $g = (2g^{\perp} + g_{||})$ = 2.12 for **1a**. The application of the same fitting procedure for other two compounds **1a–c** was not so successful: (i) the isothermal magnetization data cannot be fitted so well (ii) the g-factors were too high in comparison with the EPR data. These facts inspired us to include the HS (S = 5/2) impurity fraction (a residual HS fraction), which might originate from the defects in the solid, into the fitting procedure. In order to avoid overparametrization, the LS g-factors were fixed to g_{LS} = 2.12 for **1b** and **1c** as deduced from the EPR data, and the HS g-factors were fixed to g_{HS} = 2.0, which is the expected value for the $3d^5$ electronic configuration within the pseudo-octahedral geometry. Now, the fitting procedure was successful and resulted in the parameters listed in Table 4 (see also ESI,† Fig. S3). The strength of the antiferromagnetic exchange increases from the iodido-complex **1c** to chlorido-complex **1a**, which is in agreement with the structural observations.

Secondly, a two-dimensional network model was tested to evaluate the intermolecular interactions. It was simulated by a finite-size closed 4 × 4 grid of spins (see ESI,† Scheme S1) according to the following spin Hamiltonian:

Table 4 The summary of the magnetic parameters for **1a–c**[a]

Model	**1a**	**1b**	**1c**
1D chain[b]	J = −2.86 g = 2.19	J = −2.02 g = 2.12[e] x_{rHS} = 2.8%	J = −1.16 g = 2.12[e] x_{rHS} = 1.4%
2D network[c]	J = −1.79 g = 2.21	J = −1.21 g = 2.12 [e] x_{rHS} = 2.8%	J = −0.68 g = 2.12 [e] x_{rHS} = 1.6%
Ising-like[d]	Δ = 2720 r_{eff} = 17.8	Δ = 2616 r_{eff} = 32.7	Δ = 2682 r_{eff} = 210, γ = 209

[a] Values of the exchange parameter J are in cm^{-1}, values of Δ and γ are in K, r_{eff} is dimensionless; the best temperature-independent parameter χ_{TIP} values were found as: 5.2 (**1a**), 2.8 (**1b**) and 1.7 (**1c**) m^{3}mol^{-1} (SI units). [b] 1D chain according to eqn. (2). [c] 2D network according to eqn. (4). [d] Spin crossover model—see ESI† for more details. [e] g-value fixed was based on EPR analysis.

$$\hat{H} = -J\left\{\begin{array}{l}\vec{S}_1\cdot\left(\vec{S}_2+\vec{S}_4+\vec{S}_5+\vec{S}_{13}\right)+\vec{S}_2\cdot\left(\vec{S}_3+\vec{S}_6+\vec{S}_{14}\right)\\+\vec{S}_3\cdot\left(\vec{S}_4+\vec{S}_7+\vec{S}_{15}\right)+\vec{S}_4\cdot\left(\vec{S}_8+\vec{S}_{16}\right)\\+\vec{S}_5\cdot\left(\vec{S}_6+\vec{S}_8+\vec{S}_9\right)+\vec{S}_6\cdot\left(\vec{S}_7+\vec{S}_{10}\right)+\vec{S}_7\cdot\left(\vec{S}_8+\vec{S}_{11}\right)\\+\vec{S}_8\cdot\vec{S}_{12}+\vec{S}_9\cdot\left(\vec{S}_{10}+\vec{S}_{12}+\vec{S}_{13}\right)+\vec{S}_{10}\cdot\left(\vec{S}_{11}+\vec{S}_{14}\right)\\+\vec{S}_{11}\cdot\left(\vec{S}_{12}+\vec{S}_{15}\right)+\vec{S}_{12}\cdot\vec{S}_{16}+\vec{S}_{13}\cdot\left(\vec{S}_{14}+\vec{S}_{16}\right)\\+\vec{S}_{14}\cdot\vec{S}_{15}+\vec{S}_{15}\cdot\vec{S}_{16}\end{array}\right\} \quad (4)$$

$$+\mu_B g B\sum_{i=1}^{16}\hat{S}_{z,i}$$

The theoretical magnetization was calculated analogously as in the previous case, but now, the symmetry-adapted spin function formation was not necessary. Again, both the experimental datasets were analyzed simultaneously and the fitted parameters are summarized in Table 4. Fixing of g_{LS} and g_{HS} for **1b** and **1c** was done in the same way as in the previous calculations. By scaling up to the 2D model, the decrease of the isotropic exchange constants was observed. Again, the good agreement between the experimental and calculated data was achieved (Fig. 5). Therefore, we might conclude that both 1D and 2D model analyses fitted experimental data very well, which unfortunately, does not allow us to decide whether both types of the intermolecular interactions forming the quasi 2D network are magnetically important. The fitted J values could serve as minimal and maximal estimates of the primary magnetic interactions in **1a–c**.

Furthermore, the experimental magnetic data above 250 K, showing the spin crossover phenomenon, were analyzed using the Ising-like model,[27] where free parameters are: Δ—the energy difference between the HS and LS states, γ—the cooperativeness and r_{eff}—the effective degeneracy ratio of the HS and LS states (see details in ESI†). In the case of compounds **1a** and **1b**, only two parameters Δ and r_{eff} were sufficient to properly describe the increase of the effective magnetic moment up to 450 K. For the latter compound, it was necessary to incorporate also the γ parameter—Table 4. Because none of the compounds reached the 100% HS limit up to 450 K, the found parameters may be considered as roughly estimated only. Nevertheless, the decrease in the calculated critical temperatures T_C = 945, 750 and 502 K (x_{HS} = 0.5) for **1a–c**, is in agreement with the observed trend of the effective magnetic moments, see Fig. 5.

DFT calculations

Density functional theory (DFT) calculations were performed in order to optimize the molecular geometry of the [Fe(4OH-L6)]$^+$ cation in vacuum with the aim to evaluate the molecular geometry of the complex cation non-affected by intramolecular non-covalent contacts in both the HS and LS state. As already mentioned above, the spin-state of [Fe(X-L6)]$^+$ seems to be dependent on the geometry of the cation.[9,28] The optimization procedures provided the results which are in agreement with the following hypothesis: the LS structure of the [Fe(4OH-L6)]$^+$ cation has a "tighter" ligand conformation with α parameter at value (65.3°) typical for the LS compounds, while the HS cation was optimized to have a more distorted geometry having α = 80.8° (Table 5). The metal–ligand bond lengths are similar to those observed in the solid state.

With the aim to compare the DFT obtained chromophore bond lengths, the Crystallographic Structural Database (CSD, version 1.14, 2011) was used to extract information about the [Fe(X-L6)]$^+$ complexes. Only the X-ray structures of pure LS and HS compounds were included into the analysis in order to avoid a contamination of the data set with bond lengths affected by the presence of a residual different spin-state fraction possibly present in SCO compounds. The analysis resulted in average values of the Fe–N$_{am}$, Fe–N$_{im}$, Fe–O bond lengths either in the LS or HS state, which are shown in Table 5 and the details of the calculation, can be found in ESI.†

Both HS and LS DFT-optimized geometry possesses slightly longer Fe–N$_{am}$ and Fe–N$_{im}$ bond lengths than found in the solid state—the discrepancy is about *ca.* 0.05 Å (LS) and 0.06 Å (HS) for the Fe–N$_{am}$ bonds; 0.03 Å (LS) and 0.01 Å (HS) for the Fe–N$_{im}$ bonds. The Fe–O bond lengths show the smallest difference—below 0.01 Å in both spin states. The angular distortion of the octahedron Σ is slightly higher than the solid state average in the optimized geometry of the LS form, contrary to the HS form, where the Σ parameter from the optimized geometry is significantly lower with respect to the solid state average (Table 5). Both values of the Σ parameter originating from the calculation fall into the ranges typical for the LS or HS geometries of the [Fe(X-L6)]$^+$ compounds, even if they are at the upper (LS) or lower (HS) border (see ESI,† Table S4 and ref. 9 and 28).

Conclusions

A series of three isomorphic [Fe(4OH-L6)]X (X = Cl$^-$, **1a**, Br$^-$, **1b**, I$^-$, **1c**) complexes is reported. The crystal structure of these compounds is rich on non-covalent contacts (hydrogen bonding, π–π interaction) between the discrete mononuclear cations and halide anions. The anion substitution and subsequently, the changes in the anionic volume, electronegativity and polarizability of the anions resulted in prolonging of these contacts with the increasing anionic volume (Table 2, Fig. 3).

Magnetic properties were studied in order to clarify the impact of the intermolecular interactions on the magnetic behaviour of SCO compounds. In the temperature range of 2–300 K no

Table 5 The summary of the bond lengths for the optimized geometries of the [Fe(4OH-L6)]$^+$ cation in the LS and HS states and their comparison with those determined from X-ray analyses.

S	d(Fe–N)$_{am}$/Å	d(Fe–N)$_{im}$/Å	d(Fe–O)/Å	α/°	Σ^a
1/2	2.057	1.964	1.875	65.3	48.1
5/2	2.268	2.136	1.910	80.8	85.0
LS (CSD)^b	2.007	1.936	1.883	—	47.1
HS (CSD)^c	2.205	2.117	1.920	—	98.2

^{a} Octahedral distortion calculated as $\sum_{i}^{12} = |90 - \alpha_i|$, where α_i stands for 12 *cis* angles of the coordination polyhedron. ^{b} Average bond length values for each bond pair typical for the LS [Fe(X-L6)]$^+$ compounds. ^{c} Average bond length values for each bond pair typical for the HS [Fe(X-L6)]$^+$ compounds.

obvious signs of the SCO phenomena were detected. At low temperatures significant deviations from Curie-Weiss law and Brillouin function in magnetic behaviour was observed. These deviations from the ideal paramagnetic behaviour originated from the presence of the antiferromagnetic exchange interaction and they cannot be explained on the standard basis, using a molecular field correction parameter. With no present covalent exchange pathway, it has to be concluded that the magnetic exchange interaction is mediated by intermolecular non-covalent contacts. Nevertheless, with all available data and used analytical and theoretical methods we are not able to judge which contact, with respect to the overall magnetic exchange interaction, dominates. However, there are some remarks, which must be taken into account:

a) the results of the 1D closed ring model and 2D 4 × 4 grid model are more or less the same and the magnetic dimensionality of the system cannot be distinguished

b) the antiferromagnetic interaction found in compounds **1a–c** is not constant, the $|J|$ value decreases in the sequence of **1a** (Cl^-) > **1b** (Br^-) > **1c** (I^-) (Table 4)

c) remarkably, the centroid–centroid distances of the ring–ring stacking interactions and donor–acceptor distances of the OH···X hydrogen bonds show a similar variance and both contacts prolong (Fig. 3, Table 2) in the same sequence as J. Therefore, it might be expected that both contacts are predominantly responsible for the mediation of the exchange interaction. This assumption can be supported by several literature references. Mediation of the magnetic exchange interaction *via* the ring–ring stacking interaction has been evaluated for organic radicals[29] mostly, but also this kind of the exchange interaction has been found for polynuclear complexes.[30] The hydrogen bonds are well known mediators of intermolecular magnetic interactions, especially in molecule-based magnets with long-range ordering and their role can be accentuated in molecular magnetic sponges.[31]

d) SCO was for the very first time observed in the group of the $[Fe(X\text{-}L6)]^+$ derivatives with the "tight" geometry of the hexadentate ligand (α(**1a–c**) = 62–63°) and the transition occurs above room temperature in all three cases. This suggests that such a ligand conformation favours the LS state and along with the rigid system of hydrogen bonds[32] leads to the increase of the SCO enthalpy causing a consequent shift of T_C to higher temperatures. The preference of the 4OH-L6 ligand tight geometry in the LS $[Fe(4OH\text{-}L6)]^+$ compounds was also supported by the DFT optimization of the molecular geometry in vacuum (Table 5).

e) the transition SCO temperature decrease in the series of **1a–c** with the increasing volume of the anion (Cl^-–Br^-–I^-) which was also observed for other SCO systems.[33] Despite the thorough quantitative analysis of the intermolecular interactions in **1a–c**, the detailed investigation of their impact on spin crossover properties, especially on the cooperativeness, is hindered by incompleteness of SCO.

Experimental

All reagents and solvents were purchased from commercial sources (Sigma Aldrich) and used as received. Elemental analysis was carried out on a Flash EA 1112, ThermoFinnigan. FTIR spectra were measured with an ATR setup (Magna FTIR 750, Nicolet) in the 4000–400 cm^{-1} region. EPR spectra were recorded on a MiniScope MS200 spectrometer (Magnettech) at liquid nitrogen (~77 K) and at room temperature; DPPH (2,2-diphenyl-1-picrylhydrazyl) was used as a standard.

Synthesis of [Fe(4OH-L6)]Cl (1a) and [Fe(4OH-L6)]Br (1b)

Both complexes were prepared in a similar way: 2.8 g of 4-hydroxy-salicylaldehyde was mixed with 1.5 g of triethylenetetramine in 50 ml of methanol. Immediate formation of a yellow precipitate was observed. After 5 min of stirring, 2.7 g of $FeCl_3.6H_2O$ (**1a**), or 3 g of $FeBr_3$ in 30 ml of methanol, was added to the ligand suspension. The reaction mixture was refluxed for 2 h (the yellow precipitate in the reaction mixture could be observed for the first 60 min). Then the solution was filtered through a paper filter and left to cool down and to evaporate slowly. After approximately one day the dark blue microcrystalline product was isolated (yields: 85% for **1a**, 81% for **1b**). Single-crystals suitable for X-ray diffraction experiments were obtained by the slow diffusion of diethyl ether into the methanolic solution of complexes. **1a**: Found: C, 50.2; H, 5.2; N, 11.7. $C_{20}Cl_1Fe_1H_{26}N_4O_4$ (M = 475.73) requires C, 50.5; H, 5.1; N, 11.7%. IR mid: ν(N–H) = 3207 cm^{-1} (m), ν(O–H) = 3023 cm^{-1} (broad, m) , $\nu(C\text{–}H)_{aliphatic}$ = 2979, 2932, 2907, 2861 cm^{-1} (w), ν(C=N) and ν(C=C) = 1595, 1548 cm^{-1} (vs). (**1b**: Found: C, 46.0; H, 4.8; N, 10.6. $Br_1C_{20}Fe_1H_{24}N_4O_4$ (M = 520.18) requires C, 46.2; H, 4.7; N, 10.8%). IR mid: ν(N–H) = 3208 cm^{-1} (w), ν(O–H) = 3099 cm^{-1} (broad, m) $\nu(C\text{–}H)_{aliphatic}$ = 2977, 2929, 2906, 2861 cm^{-1} (m), ν(C=N) and ν(C=C) = 1593, 1547 cm^{-1}

Synthesis of [Fe(4OH-L6)]I (1c)

This compound was prepared by the anion substitution of **1a**: 0.4 g of **1a** was dissolved in 50 ml of methanol and 0.16 g of KI was added to the reaction mixture, which was refluxed for 20 min. Then the solution was filtered through a paper filter and left to cool down and to evaporate slowly. After approximately one day the brown crystalline product was isolated (yield: 44%). The product is dark blue when ground. (Found: C, 42.2; H, 4.3; N, 9.8. $C_{20}Cl_1Fe_1H_{26}N_4O_4$ (M = 567.18) requires C, 42.4; H, 4.4; N, 9.9%). IR mid: ν(O–H) = 3177 cm^{-1} (broad, m), ν(N–H) = 3222 cm^{-1} (m), $\nu(C\text{–}H)_{aromatic}$ = 3017 cm^{-1} (vw), $\nu(C\text{–}H)_{aliphatic}$ = 2976, 2925, 2905, 2859 cm^{-1} (w), ν(C=N) and ν(C=C) = 1596, 1548 cm^{-1} (vs)

Magnetic data

Magnetic susceptibility and magnetization measurements were done using a SQUID magnetometer (MPMS, Quantum Design) from T = 2 K at B = 0.1 T (temperature dependance). The magnetization data were taken at T = 2.0 and 4.6 K, respectively (field dependence from 0 to 7 T). The effective magnetic moment was calculated as usual: $\mu_{eff}/\mu_B = 798(\chi' T)^{1/2}$ when SI units are employed.

In the case of high temperature magnetic measurements (300–450 K), the experiment was carried out on an MPMS SQUID magnetometer (Quantum Design, model MPMS-XL-5) with installed special heating setup. A high temperature sample holder consisted of a quartz glass tube and Teflon filler. The very small diamagnetic contribution of the gelatine capsule and high temperature sample holder had a negligible contribution to the overall magnetization, which was dominated by the sample. The diamagnetic corrections of the molar magnetic susceptibilities were applied using Pascal's constants.[34] Analysis of magnetic data was done with the package POLYMAGNET.[35]

X-ray crystallography

Single crystal X-ray diffraction data were collected on an Oxford diffractometer Xcalibur2 with the Sapphire CCD detector and fine-focused sealed tube (Mo Kα radiation, λ = 0.71073 Å) source and equipped with an Oxford Cryosystem nitrogen gas-flow apparatus. All structures were solved by direct methods using SHELXS97[36] incorporated into the WinGX program package.[37] For each structure its space group was checked by the ADSYMM procedure of the PLATON[38] software. All structures were refined using full-matrix least-squares on F_o^2-F_c^2 with SHELXTL-97[36] with anisotropic displacement parameters for all non-hydrogen atoms. The hydrogen atoms were placed into the calculated positions and they were included into the riding-model approximation with U_{iso} = 1.2 U_{eq} (atom of attachment). All the crystal structures were visualized using the Mercury software.[39]

Theoretical calculation

Density functional calculations were performed using the Spartan software package (Spartan10, Ver. 1.1.0)[40] The geometries of the [Fe(4OH-L6)]$^+$ complex cation were optimized both in the LS and HS state in a vacuum at the B3LYP/LACVP+* level of theory.

Acknowledgements

We acknowledge the financial support from the Grant Agency of the Czech Republic (GAČR P207/11/0841), the Operational Program Research and Development for Innovations (CZ.1.05/2.1.00/03.0058) and the Operational Program Education for Competitiveness (CZ.1.07/2.3.00/20.0017) of the Ministry of Education, Youth and Sports of the Czech Republic; Slovak republic: VEGA 1/0052/11, APVV-0014-11; Germany: DAAD (ID50725741); Austria: Fonds zur Förderung der Wissenschaftlichen Forschung in Österreich (Project 19335-N17). We also thank Dr. Giorgio Zoppellaro for fruitful discussions concerning EPR.

References

1 L. Cambi and L. Szego, *Ber. Dtsch. Chem. Ges. B*, 1931, **64**, 2591.
2 P. Gutlich and H. A. Goodwin, *Top. Curr. Chem.*, 2004, **233**, 1.
3 (*a*) I. Šalitroš, N. T. Madhu, R. Boča, J. Pavlik and M. Ruben, *Monatsh. Chem.*, 2009, **140**, 695; (*b*) M. A. Halcrow, *Polyhedron*, 2007, **26**, 3523; (*c*) P. J. van Koningsbruggen, Y. Maeda and H. Oshio, *Top. Curr. Chem.*, 2004, **233**, 259.
4 (*a*) E. Konig and K. Madeja, *Inorg. Chem.*, 1967, **6**, 48; (*b*) E. Konig, K. Madeja and K. J. Watson, *J. Am. Chem. Soc.*, 1968, **90**, 1146; (*c*) E. W. Muller, H. Spiering and P. Gutlich, *Chem. Phys. Lett.*, 1982, **93**, 567; (*d*) A. G. Maddock and J. J. Schleiffer, *J. Chem. Soc., Dalton Trans.*, 1977, 617; (*e*) P. Ganguli, P. Gutlich, E. W. Muller and W. Irler, *J. Chem. Soc., Dalton Trans.*, 1981, 441.
5 S. Dorbes, L. Valade, J. A. Real and C. Faulmann, *Chem. Commun.*, 2005, 69.
6 C. Faulmann, S. Dorbes, J. A. Real and L. Valade, *J. Low Temp. Phys.*, 2006, **142**, 261.
7 (*a*) M. Clemente-Leon, E. Coronado, M. C. Gimenez-Lopez, A. Soriano-Portillo, J. C. Waerenborgh, F. S. Delgado and C. Ruiz-Perez, *Inorg. Chem.*, 2008, **47**, 9111; (*b*) M. Clemente-Leon, E. Coronado, M. Lopez-Jorda, G. M. Espallargas, A. Soriano-Portillo and J. C. Waerenborgh, *Chem.–Eur. J.*, 2010, **16**, 2207; (*c*) M. Clemente-Leon, E. Coronado and M. Lopez-Jorda, *Dalton Trans.*, 2010, **39**, 4903.
8 S. Floquet, S. Salunke, M. L. Boillot, R. Clement, F. Varret, K. Boukheddaden and E. Riviere, *Chem. Mater.*, 2002, **14**, 4164.
9 R. Pritchard, S. A. Barrett, C. A. Kilner and M. A. Halcrow, *Dalton Trans.*, 2008, 3159.
10 G. D'Avino, L. Grisanti, A. Painelli, J. Guasch, I. Ratera and J. Veciana, *CrystEngComm*, 2009, **11**, 2040.
11 E. Coronado, M. C. Gimenez-Lopez, C. Gimenez-Saiz and F. M. Romero, *CrystEngComm*, 2009, **11**, 2198.
12 (*a*) Y. Nishida, K. Kino and S. Kida, *J. Chem. Soc., Dalton Trans.*, 1987, 1957; (*b*) E. Sinn, G. Sim, E. V. Dose, M. F. Tweedle and L. J. Wilson, *J. Am. Chem. Soc.*, 1978, **100**, 3375.
13 J. Bernstein, R. E. Davis, L. Shimoni and N. L. Chang, *Angew. Chem., Int. Ed. Engl.*, 1995, **34**, 1555.
14 C. Janiak, *J. Chem. Soc., Dalton Trans.*, 2000, 3885.
15 (*a*) G. Gilli and P. Gilli, *The nature of the hydrogen bond*, Oxford University Press, Oxford, 2009; (*b*) G. R. Desiraju and T. Steiner, *The weak hydrogen bond*, University Press, Oxford, 1999.
16 (*a*) G. Aullon, D. Bellamy, L. Brammer, E. A. Bruton and A. G. Orpen, *Chem. Commun.*, 1998, 653; (*b*) T. Steiner, *Acta Crystallogr., Sect. B: Struct. Sci.*, 1998, **54**, 456.
17 K. Nakamoto, M. Margoshes and R. E. Rundle, *J. Am. Chem. Soc.*, 1955, **77**, 6480.
18 (*a*) B. Bleaney and M. C. M. O'Brien, *Proc. Phys. Soc., London, Sect. B*, 1956, **69**, 1216; (*b*) J. S. Griffith, *The theory of transition-metal ions*, Cambridge University Press, Cambridge, 1961.
19 C. P. S. Taylor, *Biochim. Biophys. Acta, Protein Struct.*, 1977, **491**, 137.
20 S. Stoll and A. Schweiger, *J. Magn. Reson.*, 2006, **178**, 42.
21 M. S. Haddad, M. W. Lynch, W. D. Federer and D. N. Hendrickson, *Inorg. Chem.*, 1981, **20**, 123.
22 C. Gandolfi, G. G. Morgan and M. Albrecht, *Dalton Trans.*, 2012, **41**, 3726.
23 (*a*) see e.g. M. D. Timken, D. N. Hendrickson and E. Sinn, *Inorg. Chem.*, 1985, **24**, 3947; (*b*) Y. Maeda, H. Oshio, Y. Takashima, M. Mikuriya and M. Hidaka, *Inorg. Chem.*, 1986, **25**, 2958; (*c*) J. K. Beattie, *Adv. Inorg. Chem.*, 1988, **32**, 1.
24 R. Boča, *Theoretical foundation of molecular magnetism*, Elsevier: Amsterdam, 1999.
25 (*a*) Y. H. Deng, J. Liu, B. Wu, C. Ambrus, T. D. Keene, O. Waldmann, S. X. Liu, S. Decurtins and X. Yang, *Eur. J. Inorg. Chem.*, 2008, 1712; (*b*) R. Herchel, Z. Šindelář, Z. Trávníček, R. Zbořil and J. Vančo, *Dalton Trans.*, 2009, 9870; (*c*) Z. Trávníček, R. Herchel, J. Mikulík and R. Zbořil, *J. Solid State Chem.*, 2010, **183**, 1046; (*d*) I. Nemec, R. Herchel, R. Boča, I. Svoboda, Z. Trávníček, L. Dlháň, K. Matelková and H. Fuess, *Inorg. Chim. Acta*, 2011, **366**, 366.
26 O. Waldmann, *Phys. Rev. B: Condens. Matter*, 2000, **61**, 6138.
27 (*a*) A. Bousseksou, J. Nasser, J. Linarès, K. Boukheddaden and F. Varret, *J. Phys. I*, 1992, **2**, 1381; (*b*) R. Boča and W. Linert, *Monatsh. Chem.*, 2003, **134**, 199.
28 M. A. Halcrow, *Chem. Soc. Rev.*, 2011, **40**, 4119.
29 (*a*) M. Deumal, M. A. Robb and J. J. Novoa, *Polyhedron*, 2005, **24**, 2368–2376; (*b*) J. Jornet, M. Deumal, J. Ribas-Ariño, M. J. Bearpark, M. A. Robb, R. G. Hicks and J. J. Novoa, *Chem.–Eur. J.*, 2006, **12**, 3995; (*c*) A. A. Leitch, R. T. Oakley, R. W. Reed and L. K. Thompson, *Inorg. Chem.*, 2007, **46**, 6261; (*d*) J. B. Gilroy, M. T. Lemaire, B. O. Patrick and R. G. Hicks, *CrystEngComm*, 2009, **11**, 2180; (*e*) L. Norel, L. M. Chamoreau and C. Train, *Polyhedron*, 2010, **29**, 342; (*f*) J. B. Rota, B. Le Guennic and V. Robert, *Inorg. Chem.*, 2010, **49**, 1230.
30 E. Pardo, M. Verdaguer, P. Herson, H. Rousseliere, J. Cano, M. Julve, F. Lloret and R. Lescouezec, *Inorg. Chem.*, 2011, **50**, 6250.
31 (*a*) see e.g. J. Larionova, S. A. Chavan, J. V. Yakhmi, A. G. Froystein, J. Sletten, C. Sourisseau and O. Kahn, *Inorg. Chem.*, 1997, **36**, 6374; (*b*) O. Kahn, J. Larionova and J. V. Yakhmi, *Chem.–Eur.*

J., 1999, **5**, 3443; (*c*) R. Herchel, J. Tuček, Z. Trávníček, D. Petridis and R. Zbořil, *Inorg. Chem.*, 2011, **50**, 9153.
32 All of the LS [Fe(X-L6)]+ derivatives not exhibiting SCO which were reported so far had small counter anions (halido, nitrato). These create hydrogen bonds of significant strength with the amine groups of the coordinated ligand, or with an assistance of the water molecules.
33 See *e.g.* M. M. Dirtu, C. Neuhausen, A. D. Naik, A. Rotaru, L. Spinu and Y. Garcia, *Inorg. Chem.*, 2010, **49**, 5723.
34 O. Kahn, *Molecular Magnetism*, 1993, VCH Publishers New York.
35 R. Boča, *Program POLYMAGNET. STU Bratislava*, 2008.
36 G. M. Sheldrick, *Acta Crystallogr., Sect. A: Found. Crystallogr.*, 2008, **64**, 112.
37 L. J. Farrugia, *J. Appl. Crystallogr.*, 1999, **32**, 837.
38 (*a*) A.L. Speck, "*PLATON, a multipurpose crystallographic tool.*" Utrecht University, Utrecht, The Netherlands, 2001; (*b*) Y. Le Page, MISSYM1.1 - a flexible new release, *J. Appl. Crystallogr.*, 1988, **21**, 983.
39 C. F. Macrae, P. R. Edgington, P. McCabe, E. Pidcock, G. P. Shields, R. Taylor, M. Towler and J. van de Streek, *J. Appl. Crystallogr.*, 2006, **39**, 453.
40 Spartan10, Ver. 1.1.0, Wavefunction, Inc., 2010.